Applied Catalysis B: Environmental 97 (2010) 49–56

Contents lists available at ScienceDirect

Applied Catalysis B: Environmental

journal homepage: www.elsevier.com/locate/apcatb

Novel mesoporous zirconia-based catalysts for WGS reaction

Joanna Goscianska[a], Maria Ziolek[a,*], Emma Gibson[b], Marco Daturi[b,1]

[a] Adam Mickiewicz University, Faculty of Chemistry, Grunwaldzka 6, 60-780 Poznań, Poland
[b] Laboratoire Catalyse et Spectrochimie, ENSICAEN, Université de Caen, CNRS, 6 Bd Maréchal Juin, F-14050 Caen, France

ARTICLE INFO

Article history:
Received 5 December 2009
Received in revised form 17 March 2010
Accepted 19 March 2010
Available online 25 March 2010

Keywords:
Pt/niobia–zirconia
Acidity
WGS
Formate intermediate
Operando–FT-IR/MS

ABSTRACT

Newly synthesized mesoporous zirconia-based catalysts were investigated for the WGS reaction, using niobium oxide as a promoter and platinum as the active metal. Their performances for hydrogen production were correlated to the surface properties. Niobium addition gives rise to different effects: the 0.3 loading considerably enhances the catalytic performances of the catalyst for all temperatures, for both hydrogen production and selectivity (with respect to the CO to CO_2 oxidation). On the contrary, when a Nb monolayer is produced on the zirconia surface, the activity is highly reduced with respect to the Pt/ZrO_2 sample. In particular, the acid–base behaviour of the surface was linked to the zirconia–niobia interaction and its consequence on the metal–support interaction. A description of the surface was attempted and a reaction pathway through formate species formation and decomposition proposed.

1. Introduction

The water–gas shift (WGS) process ($CO + H_2O \leftrightarrow CO_2 + H_2$) is one of the important steps in the industrial production of hydrogen [1], having gained considerable importance in recent years thanks to the quest for alternative energy transformation devices (such as fuel cells, hybrid systems, . . .) for stationary and automotive applications [2]. The WGS reaction is a critical step in fuel processors for preliminary CO clean up and additional hydrogen generation prior to the CO preferential oxidation or methanation step. WGS units are placed downstream of the reformer to further lower the CO content and improve the H_2 yield. Ideally, the WGS stage(s) should reduce the CO level to less than 5000 ppm. To achieve this low limit in CO when produced from reformate, the WGS catalyst has to be active at low temperatures, 200–280 °C, depending on the inlet concentrations of reformate. The reaction is slightly exothermic and can, at low temperature, result in the production of only low levels of CO, however it is limited by kinetics at low temperature, but has favourable kinetics at higher temperature [2,3].

It is well known from the literature [e.g. 4–6] that Pt-supported catalysts (mainly Pt/CeO_2) are one of the most active materials for WGS reactions at low temperature. Ceria, in particular, has been shown to be a very interesting support when loaded with a reduction promoting metal, for example: rhodium, platinum, palladium, nickel, iron, cobalt, and copper [2]. Unfortunately, the basicity of the ceria surface is the main cause for the catalyst deactivation under working conditions, via the formation of stable carbonates [7,8].

Currently, there are two prominent lines of thought on the role of ceria and the metal in the WGS reaction mechanism [2]. Bunluesin et al. [9] have recently proposed the ceria-mediated redox process, where ceria oxidises the CO adsorbed on the metal. After which, the ceria is reoxidised by water. The rate of the WGS reaction is thought to be controlled by both the oxygen transfer from ceria to the metal and the reoxidation of the ceria. Shido and Iwasawa [10] previously proposed the surface formate mechanism. In this case, CO reacts with surface geminal OH groups on the ceria surface producing formates which could then act as intermediates. H_2 and CO_2 are formed by the subsequent decomposition of the formates, the latter through the formation of unidentate carbonates.

It is not excluded that both mechanisms can take place on a catalyst, depending on the physico-chemical properties of the material, i.e. its redox ability, acidity, basicity, metal–support interaction, etc.

In this work the focus was on new promising platinum catalysts based on niobia/zirconia supports. On one side, we try to contribute to the discussion on the WGS mechanism, zirconia support being almost irreducible in the conditions investigated. On the other hand, as our support is essentially acidic, we also try to overcome the problem concerning the formation of poisons, such as carbonates.

* Corresponding author. Tel.: +48 618291243.
E-mail addresses: ziolek@amu.edu.pl (M. Ziolek), Marco.Daturi@ensicaen.fr (M. Daturi).
[1] Tel.: +33 231452730.

0926-3373/$ – see front matter © 2010 Elsevier B.V. All rights reserved.
doi:10.1016/j.apcatb.2010.03.023

2. Experimental

2.1. Sample preparation

For the preparation of meso- and macro-porous zirconia a typical procedure described in Ref. [11,12] was used. A 15 wt.% micellar solution of cetyltrimethylammonium bromide (CTMABr) was prepared by dissolving CTMABr (Aldrich) in an aqueous acidic solution (HCl, pH 2) at 40 °C whilst stirring for a minimum of 3 h. An appropriate quantity of zirconium propoxide ($Zr(OC_3H_7)_4$) was added dropwise into the above solution at the surfactant/Zr molar ratio of 0.33. After further stirring for 1 h at room temperature, the mixture was transferred into a polypropylene bottle, and heated in an oven at 60 °C for 48 h. The sample was calcined in air at 400 °C for 4 h.

NbO_x/ZrO_2 samples were prepared by incipient wetness impregnation of ZrO_2 with trisoxalate ammonium complex of niobium (CBMM, Brazil). Nb surface densities were calculated on the basis of the surface area of the zirconia support (84 m^2/g). The nominal monolayer coverage was calculated assuming that the cross-section of the Nb_2O_5 unit occupies a surface of 0.32 nm^2 [13]. The solids were then dried at 100 °C for 5 h and calcined in air for 5 h at 400 °C. Such prepared materials (supports for platinum) are denoted as: $0.3Nb/ZrO_2$ (0.3 monolayer of Nb-species) and $1Nb/ZrO_2$ (1 monolayer of Nb-species).

Incipient wetness technique was used to impregnate all the materials with an aqueous solution of hexachloroplatinic acid ($H_2PtCl_6 \cdot H_2O$, Aldrich) in the amount necessary to obtain 1 wt.% Pt loading. The catalysts were successively dried at 100 °C for 5 h (temperature ramp 12 °C min^{-1}) and calcined in air for 3 h at 400 °C (temperature ramp 2 °C min^{-1}) and reduced in 5% $H_2 + N_2$ flow at 500 °C for 3 h.

2.2. Sample characterisation

The prepared materials were characterised by X-ray diffraction (XRD) using a D8 Advance diffractometer (Bruker) (CuKα radiation, λ = 0.154 nm).

Surface areas, pore diameters and pore volumes of the samples were calculated from low temperature nitrogen adsorption isotherms measured on a Micromeritics 2010 sorptometer. Prior to adsorption measurements, the samples were degassed in vacuum at 300 °C for 3 h.

TEM and SEM studies were performed using a JEOL 2000 electron microscope operating at 80 and 15 kV, respectively. Powdered samples were deposited on a grid with a perforated carbon film before being transferred to the electron microscope.

UV–vis spectra were recorded using a Varian-Cary 300 Scan UV–vis spectrophotometer. Catalyst powders were placed into the cell equipped with a quartz window. The Kubelka–Munk function ($F(R)$) was used to convert reflectance measurements into equivalent absorption spectra using the reflectance of SPECTRALON as a reference.

The oxidation state of the metals was estimated from XPS measurements which were performed on a VSW apparatus (Vacuum Systems Workshop Ltd. England).

2.3. In situ IR analysis

Material surface properties have been studied by in situ FT-IR spectroscopy of adsorbed probe molecules. Self-supporting pellets of around 10 mg cm^{-2} were prepared and analysed in a classical quartz cell connected to a vacuum-adsorption apparatus for in situ experiments. Spectra were either recorded at liquid nitrogen or room temperature with a Nicolet Magna 550 FT-IR spectrometer (resolution 4 cm^{-1}). All the samples were activated in situ at 400 °C under vacuum before any characterisation.

Table 1
Platinum dispersion calculated from CO adsorption at room temperature.

Catalyst	Pt dispersion, %
Pt/ZrO_2	75
Pt/Nb_2O_5	11
$Pt/0.3Nb/ZrO_2$	63
$Pt/1Nb/ZrO_2$	91

For the analysis of platinum dispersion (calculated from FT-IR spectra of CO adsorbed at room temperature) samples were treated three times with hydrogen and vacuum (~10^{-4} Pa) at 300 °C for 1.5 h, prior to adsorption of small doses of CO (0.04–7.75 mmol).

The presence of Brønsted acid sites was investigated by the adsorption of CO at low temperature. The cell was placed in a Dewar of liquid nitrogen, reaching approximately −173 °C prior to the adsorption of small doses of CO, this was followed by dynamic evacuation.

2.4. Operando IR analysis

An *operando* system already described elsewhere [14] was used to test the sample activity for the WGS reaction. The materials were pressed into self-supporting wafers of around 10 mg cm^{-2} and placed into a steel reactor. IR analyses were carried out with a Nicolet FT-IR Nexus spectrometer equipped with a MCT detector. The analysis of the outlet gases was performed by means of a Pfeiffer Omnistar mass spectrometer. Likewise FT-IR spectra of the gas phase were collected using a gas microcell. The sample was activated in situ at 400 °C over 3 h under a flow of 10% O_2 in Ar. Reaction temperatures ranged from 50 to 400 °C, while the total flow was fixed at 25 cm^3 min^{-1}. Reactant concentrations were 1% CO and 1% water in Ar.

3. Results and discussion

3.1. Structural and surface characterisations

Structural and textural characteristics of the catalysts applied in this work have already been published in [15] and will be only briefly recalled here.

The parent materials are meso- and macro-porous and exhibit surface areas of about 80 m^2/g. The impregnation of zirconia with niobium salt and chloroplatinic acid only slightly influences the textural features (surface area and pore volume decrease). SEM images indicated a crystalline material and TEM results revealed well ordered mesopores in all supports used for platinum. The X-ray diffraction patterns of the calcined supports (zirconia and niobia–zirconia) exhibited mainly the tetragonal phase of zirconia. Comparison of XRD patterns of ZrO_2, $0.3Nb/ZrO_2$, $1Nb/ZrO_2$ indicated small changes after NbO_x loading, but they did not allow us to clearly estimate the presence or the absence of the NbO_x crystal phase. However, the presence of such species was confirmed by the UV–vis study, which provided evidence of the chemical interaction of Nb_2O_5 with the ZrO_2 support or isolation of Nb-species partially included into the zirconia structure. Such a strong interaction was also highlighted by XPS spectra, which also showed the dominance of platinum cationic species in the niobium containing samples. This behaviour was confirmed by CO adsorption followed by IR spectroscopy, also exhibiting characteristics of tetragonal zirconia on the original support.

Pt dispersion was quantified by CO adsorption at room temperature, as reported in Table 1.

Bulk niobium oxide exhibits a low surface area (3 m^2/g) and therefore Pt dispersion is very low (11%). On the contrary meso-

and macro-porous zirconia (60% of mesopores and a surface area of 84 m^2/g) gives a 75% dispersion of platinum. Interestingly, the 0.3 monolayer of NbO_x loaded on ZrO_2 leads to the decrease in Pt dispersion (to 63%), whereas the monolayer of NbO_x on ZrO_2 significantly enhances the Pt dispersion (to 91%). These results suggest that in the case of binary oxides (Nb and Zr oxides), as supports for platinum, ZrO_2 is the preferential platinum location when a 0.3 monolayer of NbO_x is used. Platinum located on the zirconia surface, in the holes between NbO_x islands, agglomerates easily on heating. In contrast, when the monolayer of NbO_x is applied, platinum is loaded on niobium oxide and because of the SMSI behaviour of niobium oxides [16], the sintering effect on heating is negligible. Therefore, high dispersion of Pt is reached if NbO_x is loaded as a monolayer. These results can be very important for the interpretation of the catalytic activity of these samples, aiding in the understanding of one of the roles of niobium promotion, which here is found to influence the metal dispersion.

Acid–base properties of the prepared catalysts were measured by the use of complementary methods such as the FT-IR study of the adsorption of probe molecules (pyridine, CO and CO_2) in conjunction with test reactions (dehydration of isopropanol—i-PrOH, and cyclization of acetonylacetone—AcoAc). Pyridine adsorption was used to probe Lewis and Brønsted acidity (LAS and BAS) and for the same purpose the low temperature (−173 °C) adsorption of CO was performed, whereas CO_2 adsorption probed Lewis basicity (LBS). AcoAc transformation was used to test for Brønsted acid and basic centres and 2-PrOH decomposition were used to detect Lewis basicity as well as BAS/LAS.

The results of the test reaction (AcoAc) and study of the adsorption of pyridine followed by FT-IR clearly indicated the difference in acid–base properties depending on NbO_x loading. Pure zirconia exhibited hydroxyl basicity ($OH^{\delta-}$) estimated from the MCP/DMF ratio in acetonylacetone cyclization. Moreover, Lewis acid centres were observed on its surface (pyridine, CO adsorption at RT and −173 °C). Globally, the surface of zirconia can be described as in Fig. 1.

Introduction of NbO_x species on the zirconia surface reduces the number of LAS because of the chemical interaction of zirconia Lewis acid sites and NbO_x entities. Moreover, changes in the MCP/DMF ratio result from the reduction of hydroxyl basicity. These effects increase with NbO_x loading. This finding suggests that NbO_x species are located near both hydroxyls and Lewis acid sites, which chemically interact with niobium species [15].

Such chemical interaction not only reduces the effectiveness of OH basic sites and ZrO_2 Lewis acid site activity but also generates active oxygen atoms at the interface between the NbO_x and ZrO_2 phases. This phenomenon is well observed on 0.3Nb/ZrO_2 with carbonate and hydrogen-carbonate formation after CO adsorption at RT [15]. Carbonates are generated with the participation of active oxygen atoms from NbO_x species which are linked to ZrO_2, whereas the formation of hydrogen-carbonates requires the presence of a hydroxyl group from the zirconia surface. Carbonates are not formed on pure ZrO_2 and they are only slightly visible on 1Nb/ZrO_2. Zirconia does not possess centres containing active oxygens necessary for carbonate formation, while active oxygens appear on the corners formed between NbO_x crystallites and the zirconia support. A monolayer of NbO_x on ZrO_2 eliminates (or significantly reduces) the number of these corners. In such a way it reduces the places where active oxygens are generated. This explains the fact that a very low concentration of carbonates was formed upon CO adsorption on 1Nb/ZrO_2. Further generation of hydrogen-carbonates observed on 1Nb/ZrO_2 suggests that a portion of $OH^{\delta-}$ groups from ZrO_2 are not totally covered by the NbO_x monolayer.

The above considerations allow us to propose the following models of 0.3Nb/ZrO_2 and 1Nb/ZrO_2 systems reported in Fig. 1.

It is of interest to stress that both the Lewis and Brønsted acidity found on the investigated samples are highly modified by the NbO_x species. In particular, niobium is known to be a promoter of Brønsted acidity [16,17], therefore the analysis of the latter merits greater attention on such samples. To have a more reliable view on the nature and on the concentration of the LAS and BAS than that

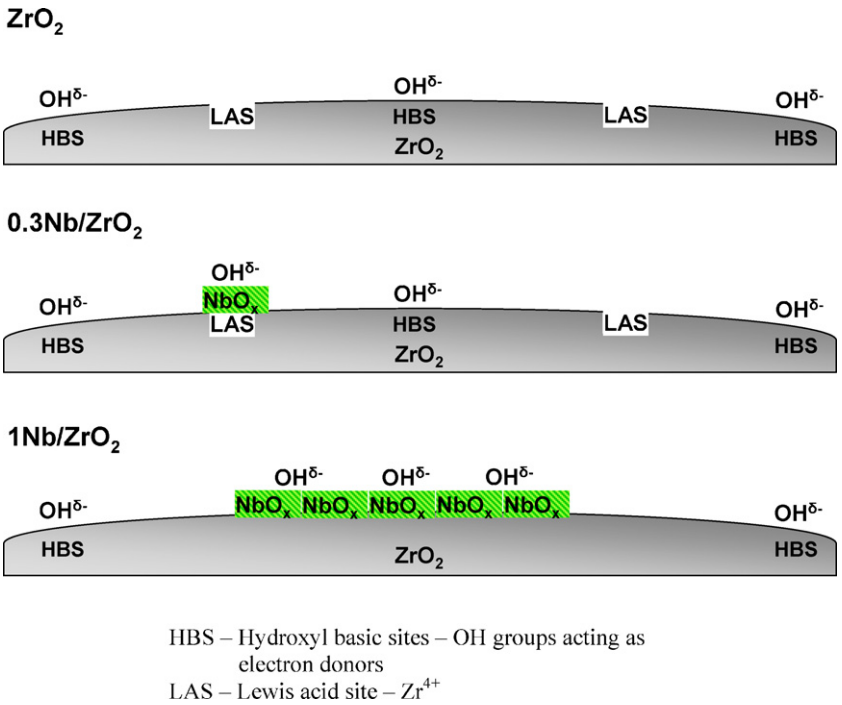

Fig. 1. Proposed simplified model of the zirconia sample and ZrO_2 supporting niobium oxide as resulting from spectroscopic and catalytic tests for acid–base properties [14]. NbO_x moieties are correlated with the presence of LAS (Lewis acid sites—Zr^{4+}) behaving as anchoring sites for the Nb entities, and with the formation of hydroxyl groups from the basic surface oxygen atoms.

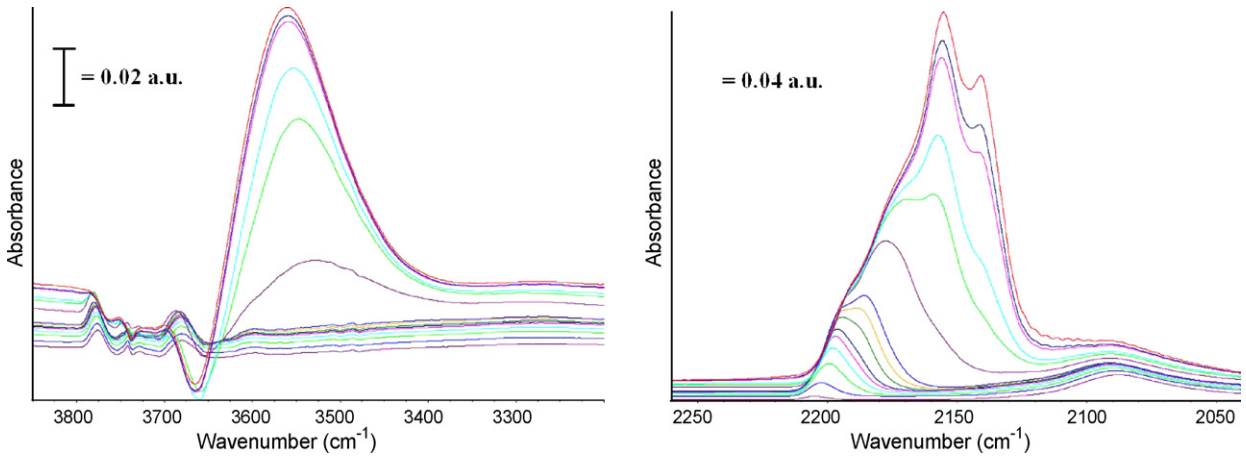

Fig. 2. IR spectra of increasing CO doses (0.12–12 μmol, then 133 Pa equilibrium pressure) on the activated Pt/0.3Nb/ZrO_2 sample at −173 °C. Left side: region of the ν(OH) vibrations; right site: region of the ν(CO) vibrations.

given by pyridine adsorption, we have followed the adsorption of small doses of CO, at about −173 °C, by IR spectroscopy. In general, CO addition at −173 °C leads to the emergence of three regions that are due to ν(CO) bands (i) the 2235–2180 cm^{-1} region, arising from Lewis acid sites, (ii) the 2180–2150 cm^{-1} region, arising from Brønsted acid sites but also weak Lewis acid sites, and (iii) the region <2150 cm^{-1} due to physisorbed species and to the carbonyls on Pt clusters (below 2100 cm^{-1}) [18]. The ν(CO) position is a function of acid strength, the higher the wavenumber, the stronger is the acidity. A correlation between the ν(OH) and ν(CO) regions is required to define the nature of the CO interaction, for example via coordination or via H bonding with hydroxyl groups, to distinguish Brønsted acidity from weak Lewis acidity in the 2150–2180 cm^{-1} range [19]. A typical spectral evolution of the ν(CO) region for the investigated samples is given in Fig. 2, where Pt/0.3Nb/ZrO_2 has been taken as an example. At the first CO doses only the strongest LAS are revealed by CO adsorption (band at 2205 cm^{-1}). Adding increasing doses of the probe molecule, new species appear at 2179, 2172, 2157 and 2141 cm^{-1}, the latter being due to physisorbed species [18]. Looking carefully at the spectra both in the ν(OH) and ν(CO) regions, we observe that the appearance of the 2157 cm^{-1} feature is concomitant with an important perturbation of the bridged OH groups near 3665 cm^{-1} [20,21], giving rise to a hydrogen bonding species (broad band centred at ∼3530–3560 cm^{-1}), a clear indication of the presence of a BAS. These results (ν(CO) positions and Δν(OH) shifts of ∼100–130 cm^{-1}) are coherent with a weak acidity, as already observed by Morterra et al. on similar compounds [22]. A complete view on the Lewis and Brønsted acid sites characterised by the ν(CO) vibrations at −173 °C is presented in Table 2.

Pure zirconia presents originally two LAS. On the basis of the considerations of Morterra et al. [23] these bands can be assigned to CO molecules σ-coordinated onto coordinatively unsaturated (cus) Zr^{4+} centres with differing environments on the ZrO_2 surface. The band between 2179 and 2169 cm^{-1} can be attributed to CO on (cus) Zr^{4+} centres found on extended low index planes of tetragonal ZrO_2, whereas the band at 2202–2186 cm^{-1} can be attributed to CO on (cus) Zr^{4+} centres which are found on the sides of the ZrO_2 crystallites.

It is possible to remark that, for a given site, the wavenumber decreases with the amount of introduced CO, essentially due to the fact that the strongest sites are occupied first, after which weaker sites continue to coordinate the probe molecule, giving rise to broader bands (indicating heterogeneous families of LAS or BAS), whose average position is shifted to lower wavenumbers. Comparing the different supports, we remark that Nb introduction seems to slightly increase the wavenumber (i.e. the strength) of the Lewis acid sites, while after Pt impregnation the phenomenon is enhanced and a new family of LAS is generated having a strength intermediate between the two sites already found on the supports. On the contrary, Pt introduction on pure zirconia results in the elimina-

Table 2
Position (cm^{-1}) of the different components of the ν(CO) maxima for the acid sites detected for the investigated samples by CO adsorption at −173 °C followed by FT-IR spectroscopy.

Introduced CO →	Lewis acid sites				Brønsted acid sites	
	0.12 μmol	5.88 μmol	11.76 μmol	133 Pa at equilibrium	5.88 μmol	133 Pa at equilibrium
ZrO_2	2202	2189	2188	2186	2160	2153
	–	2179	2173	2169		
Pt/ZrO_2	–	–	–	–	2157	2155
	2180 (traces)	2166	2165	2165		
1Nb/ZrO_2	2202	2190	2190	2190	∼2158	2155
	–	2177	2170	2168		
Pt/1Nb/ZrO_2	2203	2196	2194	2193	∼2159	2158
	–	2185	2182	2182		
	–	2173	2170	2167		
0.3Nb/ZrO_2	2199	2192	2190	2190	2154	2153
	–	2172	2170	2170		
Pt/0.3Nb/ZrO_2	2205	2195	2193	2193	2157	2156
	–	2179	2178	2178		
	–	2172	2171	2171		

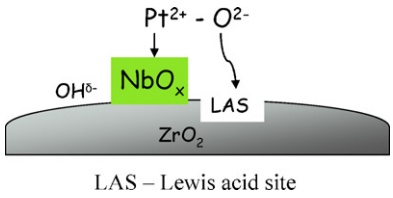

Fig. 3. Proposed simplified model of the zirconia sample supporting niobium oxide and platinum, as resulting from spectroscopic evidence [14]. Synergic interactions between supported oxidised platinum entities with NbO_x moieties and LAS (Lewis acid sites—Zr^{4+}) are shown.

tion of the higher wavenumber sites, likely "consumed" by metal grafting. BAS, which are slightly modified after niobia addition on the zirconia support, are further increased in strength by Pt impregnation.

CO adsorption at room temperature on materials impregnated with platinum, studied elsewhere [15], show that IR spectra of Pt modified ZrO_2 and $1Nb/ZrO_2$ present bands at ~2080 and ~1850 cm^{-1} assigned to linear and bridging carbonyls of Pt^0, respectively. Moreover, the presence of Pt^{2+}–CO and Pt^{+}–CO complexes were indicated by the bands at 2205–2170 cm^{-1} and 2135–2120 cm^{-1}, respectively [18], the former features being partially superimposed to those belonging to CO carbonyls on the support. Conversely, the spectrum of $Pt/0.3Nb/ZrO_2$ gives no indication of CO adsorbed on metallic platinum, being in line with the results of the XPS experiments showing the dominance of platinum cationic species.

The various surface properties of $0.3Nb/ZrO_2$ and $1Nb/ZrO_2$ indicated above may have an important impact on the catalytic properties of platinum grafted on both supports. As we have indicated, the oxidation state of platinum strongly depends on the nature of the supports used in this work. Niobium oxide is well known as a strong metal–support interaction agent [16,24]. Such interaction easily leads to the reduction of cationic platinum into metallic Pt. Therefore, a monolayer of NbO_x on ZrO_2 leads to the highest Pt^0 concentration. Interestingly, on the $Pt/0.3Nb/ZrO_2$ sample Pt^{2+} dominates, which can be explained by the stabilization of Pt^{2+}–O^{2-} on NbO_x species and Lewis acid sites of ZrO_2, as is proposed on the scheme illustrated in Fig. 3. Such stabilization together with the lower dispersion of Pt species (Table 1) makes the reduction of cationic platinum more difficult.

The intensities of the individual acid sites have been calculated by measuring the area of each component of the CO band after spectral decomposition. In this way, a comparison of the individual contributions to the CO band can be made between samples. An example is given using the $Pt/0.3Nb/ZrO_2$ sample in Fig. 4. The complete relative intensity of all the contributions for the acid sites can be found in Table 3.

The relative densities of the BAS are also reported in Fig. 5. It appears that Nb addition generally increases the concentration of Brønsted acid sites on the surface of the zirconia, whereas Pt loading decreases the concentration of such species, except for the Nb monolayer sample, which possesses the highest intensity.

Let us see now if such surface properties produce clear influences on the sample reactivity in the WGS reaction.

3.2. Study of the WGS reaction

The samples have been tested for the water–gas shift reaction, as indicated in Section 2: a wafer of each catalyst was introduced into the *operando* reactor-cell and activated in situ at 400 °C over 3 h under a flow of 10% O_2 in Ar. Then the reaction flow (25 cm^3 min^{-1}, containing 1% CO and 1% water in Ar as carrier gas) was sent through the reactor at temperatures ranging from 50 to 400 °C.

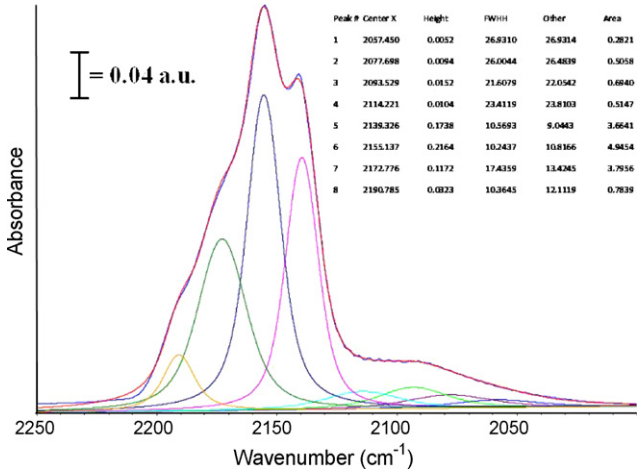

Fig. 4. Example of deconvoluted spectrum after adsorption of an equilibrium pressure of 133 Pa CO on the activated $Pt/0.3Nb/ZrO_2$ sample, at −173 °C.

Table 3
Band positions, FWHH and intensities for the different components constituting the CO adsorbed IR massif at −173 °C for all the investigated samples.

Peak #	Center *X*, cm^{-1}	Height	FWHH	Area
$Pt/1Nb/ZrO_2$				
1	2098.463	0.0214	25.5118	1.2093
2	2137.448	0.1377	7.8609	3.4632
3	2157.496	0.2529	15.9960	9.6895
4	2165.682	0.0001	21.5174	0.0030
5	2181.840	0.0819	17.1853	2.9618
6	2200.308	0.0000	20.4841	0.0000
7	2274.520	0.0047	22.1844	0.2298
$1Nb/ZrO_2$				
1	2108.070	0.0117	14.9364	0.3906
2	2138.917	0.2516	9.6582	5.3622
3	2153.750	0.2091	14.6999	6.4540
4	2170.009	0.1125	15.0806	3.5008
5	2188.205	0.0815	11.1262	1.7720
$Pt/0.3Nb/ZrO_2$				
1	2089.686	0.0263	33.1563	1.9548
2	2139.406	0.1808	8.7876	4.2123
3	2155.353	0.2245	10.7595	5.1339
4	2172.105	0.1131	16.3000	2.8034
5	2189.023	0.0506	17.9415	0.9904
6	2195.240	0.0000	12.9198	0.0000
$0.3Nb/ZrO_2$				
1	2117.408	0.0040	12.8030	0.1129
2	2139.406	0.1620	9.6359	3.5061
3	2152.068	0.3506	9.8964	8.1248
4	2168.334	0.0854	12.8765	2.3856
5	2187.287	0.0294	10.9361	0.7113
Pt/ZrO_2				
1	2103.168	0.0046	13.4251	0.1273
2	2135.211	0.0331	13.2633	0.9289
3	2153.178	0.3955	13.6163	8.5420
4	2166.394	0.0001	13.5586	0.0027
ZrO_2				
1	2104.546	0.0122	13.9945	0.3794
2	2139.661	0.3215	10.7479	6.9698
3	2152.625	0.3681	9.4377	7.2175
4	2170.101	0.2572	11.6068	5.5840
5	2186.808	0.2275	13.6494	3.4122
5.88 μmol Pt/ZrO_2				
1	2111.754	0.0016	19.8474	0.0716
2	2134.279	0.0055	18.5223	0.2214
3	2156.953	0.0895	24.6334	2.3496
4	2165.799	0.0065	10.6486	0.1537
5	2177.332	0.0017	14.0280	0.0538

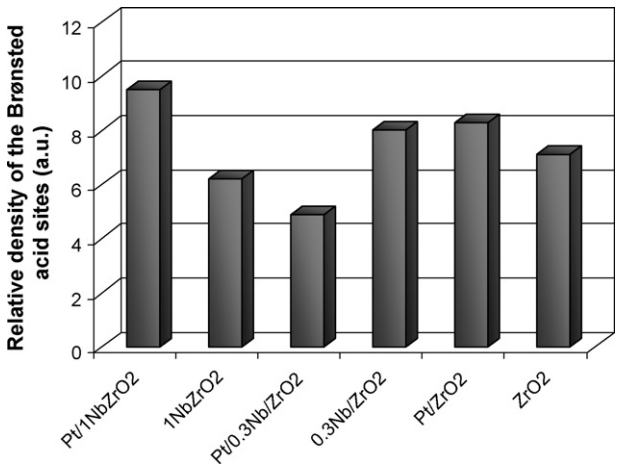

Fig. 5. Relative density of the Brønsted acid sites on the different samples (values are given in arbitrary units), as tested by CO adsorption at −173 °C followed by IR spectroscopy.

The activity of the supports was found to be negligible, while all the Pt-containing materials were more or less active for the WGS reaction, starting from 250 °C, as shown by well matching gas IR and MS analyses. The performances of the three samples are reported in Fig. 6 and Table 4: it clearly appears that Pt–ZrO_2 reactivity is already interesting and can be compared to the results found by Chenu et al. [25].

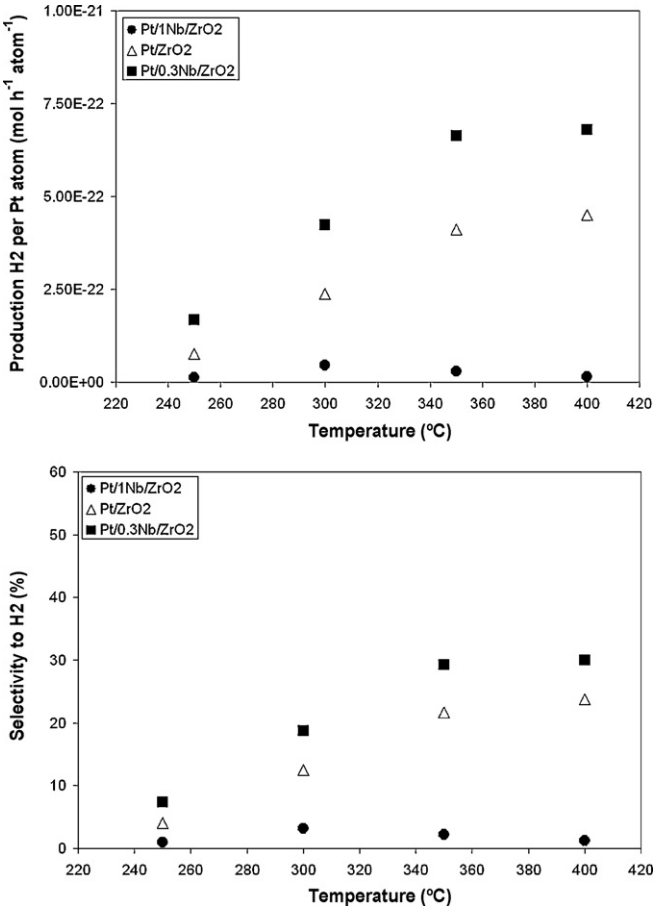

Fig. 6. Comparison of hydrogen yield on the different Pt-loaded samples (top) and hydrogen selectivity of the reaction (bottom) calculated as H_2 produced/H_2O introduced ratio.

Table 4
Hydrogen yield and selectivity for the WGS reaction on the Pt-loaded samples.

	Pt/ZrO_2	$Pt/0.3Nb/ZrO_2$	$Pt/1Nb/ZrO_2$
H_2 (mol/h/atom$_{Pt}$)			
400 °C	4.51E−22	6.79E−22	1.43E−23
350 °C	4.11E−22	6.63E−22	2.91E−23
300 °C	2.37E−22	4.24E−22	4.48E−23
250 °C	7.61E−23	1.67E−22	1.31E−23
H_2 selectivity (%)			
400 °C	23.76	29.98	1.17
350 °C	21.64	29.27	2.25
300 °C	12.45	18.75	3.22
250 °C	4.00	7.40	0.99

Niobium addition gives rise to different effects: the 0.3 loading considerably enhances the catalytic performances of the catalyst for all temperatures, for both hydrogen production and selectivity (with respect to the CO to CO_2 oxidation). On the contrary, when a Nb monolayer is produced on the zirconia surface, the activity is highly reduced with respect to the Pt/ZrO_2 sample. It is interesting to try and discover which sample properties justify this behaviour. Comparing activity results, Table 4, with Table 1 and Fig. 5 it clearly appears that there is no correlation between hydrogen production in the WGS reaction and platinum dispersion or the density of BAS. We could even say that there is a reverse correlation, since the trend of the Pt dispersion and BAS intensity are opposite with respect to the catalytic activity. In the same way, it is worth remarking that there is no apparent correlation between the relative amount of the LAS and the H_2 yield for the three catalysts, as evidenced by Fig. 7. This result is more unexpected if we assume that on the Lewis acid sites water is coordinated and can dissociate, due to the presence of acid–base pairs, evidenced by the previous surface characterisations, on the samples containing niobium, especially the sample supporting a 0.3 layer [15]. Nevertheless it is important to remember that these quantitative analyses were carried out in in situ conditions, whereas under stream the catalytic surface can have a very different behaviour. We must also recall that NbO_x species were found to be located near both hydroxyls and Lewis acid sites which chemically interact with niobium species. Such chemical interaction produces active oxygen atoms located in the corners formed between the two phases (NbO_x and ZrO_2) especially on the $0.3Nb/ZrO_2$ sample. These active oxygens are in close proximity to the zirconia support which itself possesses basic hydroxyl groups.

These considerations (which explain the water activation phenomenon) should be incorporated with the mechanism for the activation of CO, in order to be able to draw a complete reaction pathway for the WGS reaction on our samples.

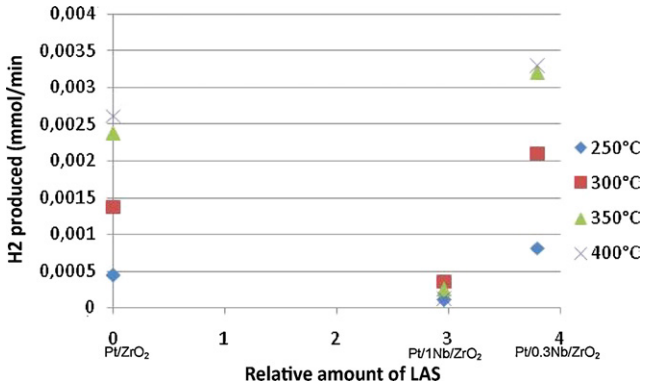

Fig. 7. Correlation between the density of the LAS and the hydrogen production for the Pt-loaded samples.

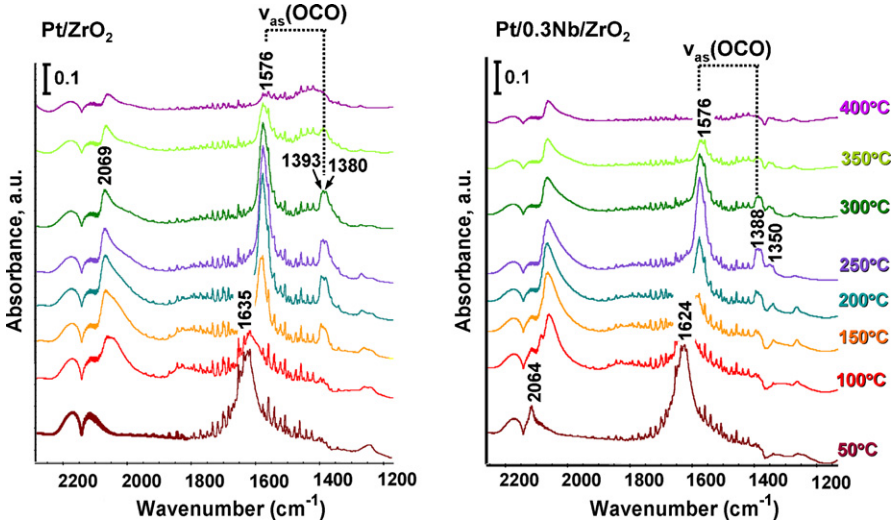

Fig. 8. FT-IR surface spectra of Pt/ZrO_2 and $Pt/0.3NbZrO_2$ in the formate vibration region.

In situ experiments, reported above, already indicated clear differences between these samples, showing the ability of the $Pt/0.3Nb/ZrO_2$ sample to stabilize Pt^{2+} entities. But what about under reaction stream? Looking at the IR spectra of the surfaces of Pt/ZrO_2 and $Pt/0.3Nb/ZrO_2$ recorded under flow of CO and water vapour during the *operando* tests (Fig. 8) we observe the bands from chemisorbed H_2O (~1630 cm^{-1}) disappearing above 100 °C, when formate species start to be formed, likely through CO linearly adsorbed on metallic Pt (~2068 cm^{-1}), well visible at 50 and 100 °C. Their intensity is greatest on the $Pt/0.3Nb/ZrO_2$ sample. In the corresponding hydroxyl region one can observe a band near ~3670 cm^{-1} assigned to bridged OH groups and a broad band at around 3400 cm^{-1} from hydrogen bonded species. As hypothesised above, H_2O is most probably chemisorbed on oxygen vacancies where it is dissociated and maintains a surface concentration of OH groups. At higher temperatures hydroxyls interact further with CO forming formates characterised by bands at 2980, 2891 cm^{-1} (ν(CH)), 1576 cm^{-1} (ν_{as}(OCO)), 1385 cm^{-1} (δ(CH)), 1379 cm^{-1} (ν_s(OCO)) [25,26]. The formate intensity reaches a maximum at 250 °C, at which point it starts to decrease, implying that formates react at the same temperature at which hydrogen production is observed. As proposed by Davis and co-workers [27–29] hydrogen formation is proposed to go through a process of formate formation then decomposition, generating as a side product carbonates, which subsequently desorb from the surface as CO_2 (Fig. 9). Essentially, in parallel to H_2 yield we observe hydrogen-carbonate formation (1559, 1433 and 1250 cm^{-1}), and the production of CO_2 in the gas phase (see Fig. 9).

On the contrary, no surface species are observed on $Pt/1Nb/ZrO_2$, except traces of CO adsorbed on Pt^0 (~2044 cm^{-1}) which appear at lower wavenumber, with respect to the previous samples, likely due to the back donation effect of the basic niobia. The second reacting agent, water, is not activated on this sample, due to the absence of both zirconia and niobia–zirconia interacting sites as the zirconia surface is totally covered by Nb (OH groups have in fact disappeared from the surface). Zirconia alone already presents acid–base pairs which are able to dissociate water, but H_2 production was found to be greatest over the sample containing 0.3Nb, as the Nb–Zr interaction leads to an enhanced concentration of acid–base pairs (as evidenced by in situ analysis). Brønsted sites found on the ZrO_2 surface can also participate in the production of H_2 by reaction with neighbouring adsorbed water molecules. Both these types of active sites are present on ZrO_2 and $0.3NbZrO_2$ supports but not on the $1NbZrO_2$ sample, which correlates well with their observed performance for the WGS reaction.

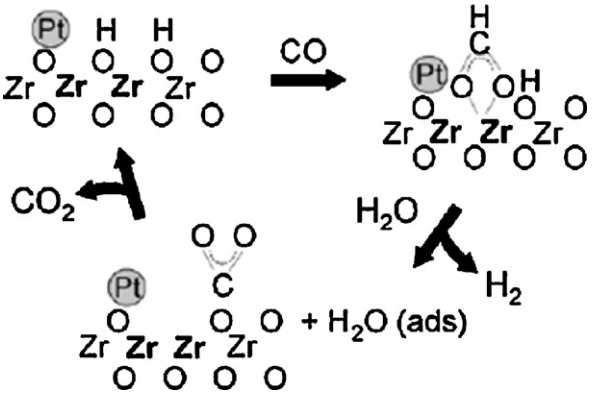

Fig. 9. Hydrogen formation via the WGS reaction as proposed by Davis et al. in Ref. [27,28].

4. Conclusions

Newly synthesized meso- and macro-porous zirconia samples have been characterised by different techniques and their performance for the WGS reaction assessed.

In particular, surface properties of the supports and Pt-loaded samples have been highlighted and discussed considering the interaction between Zr, Nb and Pt, with emphasis on the suppression, creation or modification of acid–base sites found on these samples. The surface properties of $Pt/0.3Nb/ZrO_2$ and $Pt/1Nb/ZrO_2$, discussed above, significantly influence the activity in the WGS reaction. Nevertheless, no possible correlation was observed comparing catalytic activity and surface properties measured by in situ techniques. On the contrary, the *operando* approach has presented the only way to explain sample activities. In fact, adsorbed species have been observed under *operando* conditions which corroborate the overall proposed pathway for the reaction, through carbonyl and formate intermediates, as reported in the literature. The presence of an acidic support surface is very interesting in view of limiting active site poisoning by carbonates, as occurs on ceria-based materials.

Acknowledgement

Polish Ministry of Science and Higher Education (grant no. N204 3735 33) is acknowledged for the financial support. E. G. is grateful to ADEME for the post-doctoral grant in the frame of the PREDIT program.

References

[1] C.H. Bartolomew, R.J. Farrauto, in: C.H. Bartolomew, R.J. Farrauto (Eds.), Fundamentals of Industrial Catalytic Processes, Wiley, Hoboken, NJ, 2006, p. 909.
[2] G. Jacobs, L. Williams, U. Graham, G.A. Thomas, D.E. Sparks, B.H. Davis, Appl. Catal. A: Gen. 252 (2003) 107–118.
[3] A.F. Ghenciu, Curr. Opin. Solid State Mater. Sci. 6 (2002) 389.
[4] G. Jacobs, U.M. Graham, E. Chenu, P.M. Patterson, A. Dozier, B.H. Davis, J. Catal. 229 (2005) 499–512.
[5] A. Goguet, F. Meunier, J.P. Breen, R. Burch, M.I. Petch, A. Faur Ghenciu, J. Catal. 226 (2004) 382–392.
[6] C. Wheeler, A. Jhalani, E.J. Klein, S. Tummala, L.D. Schmidt, J. Catal. 223 (2004) 191–199.
[7] X. Liu, W. Ruettinger, X. Xu, R. Farrauto, Appl. Catal. B: Environ. 56 (2005) 69–75.
[8] S. Hilaire, X. Wang, T. Luo, R.J. Gorte, J. Wagner, Appl. Catal. A: Gen. 215 (2001) 271–278.
[9] T. Bunluesin, R.J. Gorte, G.W. Graham, Appl. Catal. B: Environ. 15 (1998) 107–114.
[10] T. Shido, Y. Iwasawa, J. Catal. 141 (1993) 71–81.
[11] Z.Y. Yuan, A. Vantomme, A. Leonard, B.-L. Su, Chem. Commun. (2003) 1558–1559.
[12] H.L. Tidahy, S. Siffert, J.-F. Lamonier, E.A. Zhilinskaya, A. Aboukais, Z.-Y. Yuan, A. Vantomme, B.-L. Su, X. Canet, G. De Weireld, M. Frere, T.B. N'Guyen, J.-M. Giraudon, G. Leclerq, Appl. Catal. A: Gen. 310 (2006) 61–69.
[13] T. Onfroy, G. Clet, M. Houalla, J. Phys. Chem. B 109 (2005) 14588–14594.
[14] T. Lesage, C. Verrier, P. Bazin, J. Saussey, M. Daturi, Phys. Chem. Chem. Phys. 5 (2003) 4435–4440.
[15] J. Goscianska, M. Ziolek, E. Gibson, M. Daturi, Catal. Today (2009), doi:10.1016/j.cattod.2009.10.016.
[16] I. Nowak, M. Ziolek, Chem. Rev. 99 (1999) 3603–3624.
[17] T. Onfroy, G. Clet, S.B. Bukallah, T. Visser, M. Houalla, Appl. Catal. A: Gen. 298 (2006) 80–87.
[18] K.I. Hadjiivanov, G.N. Vayssilov, Adv. Catal. 47 (2002) 307–511.
[19] D. Dambournet, H. Leclerc, A. Vimont, J.-C. Lavalley, M. Nickkho-Amiry, M. Daturi, J.M. Winfield, Phys. Chem. Chem. Phys. 11 (2009) 1369–1379.
[20] A. Clearfield, G.P.D. Serrette, A.H. Khazi-Syed, Catal. Today 20 (1994) 295–312.
[21] M. Daturi, E. Finocchio, C. Binet, J.C. Lavalley, F. Fally, V. Perrichon, J. Phys. Chem. B 103 (1999) 4884–4891.
[22] C. Morterra, G. Cerrato, V. Bolis, S. Di Ciero, M. Signoretto, J. Chem. Soc., Faraday Trans. 93 (1997) 1179–1184.
[23] C. Morterra, G. Cerrato, S. Di Ciero, Appl. Surf. Sci. 126 (1998) 107.
[24] M. Ziolek, Catal. Today 78 (2003) 47–64.
[25] E. Chenu, G. Jacobs, A.C. Crawford, R.A. Keogh, P.M. Patterson, D.E. Sparks, B.H. Davis, Appl. Catal. B: Environ. 59 (2005) 45–56.
[26] E. Finocchio, M. Daturi, C. Binet, J.C. Lavalley, G. Blanchard, Catal. Today 52 (1999) 53–63.
[27] J.M. Pigos, C.J. Brooks, G. Jacobs, B.H. Davis, Appl. Catal. A: Gen. 328 (2007) 14–26.
[28] J.M. Pigos, C.J. Brooks, G. Jacobs, B.H. Davis, Appl. Catal. A: Gen. 319 (2007) 47–57.
[29] G. Jacobs, E. Chenu, P.M. Patterson, L. Williams, D. Sparks, G. Thomas, B.H. Davis, Appl. Catal. A: Gen. 258 (2004) 203–214.